RAA 2019 Vol. **19** No. **6**, 82(8pp) doi: 10.1088/1674–4527/19/6/82

http://www.raa-journal.org *http://iopscience.iop.org/raa*

***R**esearch in*
***A**stronomy and*
***A**strophysics*

A method for aligning the plastic scintillator detector on DAMPE

Peng-Xiong Ma[1,2], Yong-Jie Zhang[3,4,5], Ya-Peng Zhang[3], Yao Li[3], Jing-Jing Zang[1], Xiang Li[1], Tie-Kuang Dong[1,2], Yi-Zhong Fan[1,2], Shi-Jun Lei[1,2], Jian Wu[1,2], Yu-Hong Yu[3], Qiang Yuan[1,2], Chuan Yue[1,5] and Zhi-Yu Sun[3]

[1] Key Laboratory of Dark Matter and Space Astronomy, Purple Mountain Observatory, Chinese Academy of Sciences, Nanjing 210008, China; *zangjj@pmo.ac.cn; xiangli@pmo.ac.cn*
[2] School of Astronomy and Space Science, University of Science and Technology of China, Hefei 230026, China
[3] Institute of Modern Physics, Chinese Academy of Sciences, Lanzhou 730000, China; *y.p.zhang@impcas.ac.cn*
[4] School of Nuclear Science and Technology, Lanzhou University, Lanzhou 730000, China
[5] University of Chinese Academy of Sciences, Beijing 100049, China

Received 2018 June 30; accepted 2018 December 5

Abstract The Plastic Scintillator Detector (PSD) onboard the DArk Matter Particle Explorer (DAMPE) is designed to measure cosmic ray charge (Z) and to act as a veto detector for gamma ray identification. To fully exploit the charge identification potential of PSD and to enhance its capability to identify gamma ray events, we develop an alignment method for the PSD. The path length of a given track in the volume of a PSD bar is derived taking into account the shift and rotation alignment corrections. By examining energy spectra of corner-passing events and fully contained events, position shifts and rotations of all PSD bars are obtained, and are found to be on average about 1 mm and 0.0015 radian respectively. To validate the alignment method, we introduce artificial shifts and rotations of PSD bars into the detector simulation. These shift and rotation parameters can be recovered successfully by the alignment procedure. As a result of the PSD alignment procedure, the charge resolution of the PSD is improved from 4% to 8%, depending on the nuclei.

Key words: instrumentation: detectors — methods: data analysis

1 INTRODUCTION

The DArk Matter Particle Explorer (DAMPE) is a space-borne mission launched by China that has operated in solar synchronous orbit at an altitude of 500 km for more than two years. The payload carried by DAMPE consists of a high-energy cosmic ray detection system equipped with four sub-detectors (Chang et al. 2017; Ambrosi et al. 2019): a Plastic Scintillator Detector (PSD) (Yu et al. 2017; Ding et al. 2018), a Silicon Tungsten tracKer-convertor (STK) (P. Azzarello et al. 2016), a BGO calorimeter (BGO) (Zheng et al. 2016) and a NeUtron Detector (NUD) (He et al. 2016). With this design, DAMPE can measure the charge, energy and incoming direction of cosmic rays. The PSD, as a thin material detector, is designed to detect the charge of a cosmic ray by measuring its energy deposition in the plastic scintillator and also serves as a veto detector to discriminate gamma rays from charged particles (Xu et al. 2018). The STK mounted below the PSD is a silicon-strip tracker with three layers of thin tungsten plates inserted below the first, second and third detection layers. With this design, high-energy gamma rays can be converted into e^+/e^- pairs and then their trajectories can be reconstructed. STK is also designed to reconstruct the trajectories and measure the total charge (Z) of cosmic-ray ions. The BGO is a three-dimensional (3D) imaging total absorption calorimeter, which is designed to measure the energy of electrons and gamma rays from a few GeV to 10 TeV and the energy of cosmic ray nuclei from 10 GeV/n to about 200 TeV/n (DAMPE Collaboration et al. 2017; Yuan & Feng 2018). The bottom sub-detector of DAMPE is NUD, designed to enhance e/p separation power by detecting neutrons generated by a hadronic shower in the BGO. The PSD is composed of 82 plastic scintillator bars

arranged into two layers. Both layers have 39 bars with a size of $824 \times 28 \times 10\,\mathrm{mm}^3$ and two edge bars with a size of $824 \times 25 \times 10\,\mathrm{mm}^3$. The two layers are orthogonal to each other. To avoid dead regions, neighboring bars in each layer are staggered by 10 mm as shown in Figure 1. Other details about the structure of the PSD detector can be found in Yu et al. (2017).

The mean energy deposition (or most probable value (MPV) of the energy deposition) of a high-energy charged particle in a PSD bar is proportional to its path length (hereafter PL) in the volume of a PSD bar. Therefore, to obtain an accurate measurement of energy deposition for a charged particle in the PSD, it is important to carry out detector alignment for all PSD bars. If a PSD bar is not located in its designed position, the measured energy spectrum of minimum ionizing particles (MIPs) returns a distorted structure due to an incorrect calculation of the PL, especially for particles that only pass through a corner (corner-passing events). Based on this fact, we develop a method to align all PSD bars using the correlation between measured energy spectra and PL.

In this paper, we will introduce the method of PSD alignment in Section 2. The validation of this method and the associated improvement in charge resolution are described in Section 3. The results and possible application of the alignment method are presented in Section 4.

2 METHODOLOGY

As mentioned previously, the energy deposition of a charged particle in a PSD bar is sensitive to its PL. Position shift or rotation of a PSD bar would cause an incorrect calculation of the PL for the charged particles and thus the measured energy spectra of MIPs may be distorted. Typically, six independent variables are needed to describe the change in position of one PSD bar, which are three rotation angles $(\theta_{yz}, \theta_{xz}, \theta_{xy})$ and three shift distances $(\Delta_x, \Delta_y, \Delta_z)$.

Due to stability of the mechanical structure in DAMPE, the shifts and rotation of PSD bars are quite tiny so that they can be treated as first-order terms. The events which cross the upper and lower surfaces of a PSD bar (fully contained) are not sensitive to the shift along the bar. At the same time, the fully contained events are distorted only weakly by shift and rotation (see in Fig. 2). Hereafter, we will refer to the fully contained events and their measured energy spectrum as "middle events" and "standard spectrum" respectively.

As shown in Figure 2, the events that cross a corner of a PSD bar are defined as "corner-passing events," which can be divided into four cases: A, B, C and D. To convert the problem of vertical rotation into a shifting problem, each physical plastic bar is divided lengthwise into 11 equal segments.

Figure 3 shows the MPV distribution of the middle events in the 902 segments (11 segments for each PSD bar, 82 bars in total). As seen from the figure, deviations of the MIP spectra between the 902 segments are minor enough, meaning that the rotation angles θ_{yz} and θ_{xz} of PSD bars are negligible based on the PL being $\frac{\Delta z}{\cos\theta}$, that is, the upper surface of one PSD bar, corresponding to the direction of the z axis in DAMPE, is orthogonal. In addition, shifts along the bar would not worsen the charge resolution. Finally, three effective variables remain in our alignment method, which are $\Delta_{x/y}$, Δ_z and θ_{xy}, hereafter written as H, V and θ_{xy} respectively.

According to the Bethe-Bloch formula, the energy deposition is proportional to the PL for a given charged particle. The precision of measuring track direction is crucial for obtaining a proper PL. According to the Geant4-based (Agostinelli et al. 2003) simulation of DAMPE, the angular resolution of a track is about 0.2 degree, and MIP events have a clear track in DAMPE, with almost no backscattered particles. Moreover, the interaction of MIP is a purely electromagnetic process, and therefore is modeled well in Geant4, justifying the choice of MIP events for the alignment analysis. In particular, we select MIP events according to the following criteria:

(1) There is exactly one track in the event;
(2) The track should have four xy points at least;
(3) Total number of hits in PSD is more than 0 and less than 4;
(4) There are less than three hits in each PSD layer;
(5) In the first three layers of BGO there are less than two hits per layer;
(6) The total energy in the first three layers of BGO is less than five times the BGO MIP energy (22.5 MeV).

With these selection criteria, we can obtain about 45 000 MIP events using one-day of flight data. The deposited energy in one PSD bar, E_{dep}, is expressed as follows

$$E_{\mathrm{dep}} = S \cdot PL(H, V, \theta_{xy}), \tag{1}$$

where E_{dep} is the deposited energy in one bar, $PL(H, V, \theta_{xy})$ is the PL as a function of the alignment variables (H, V, θ_{xy}), and S is the MPV of deposited energy per millimeter of fully contained events in Figure 2, which is treated as the "standard value."

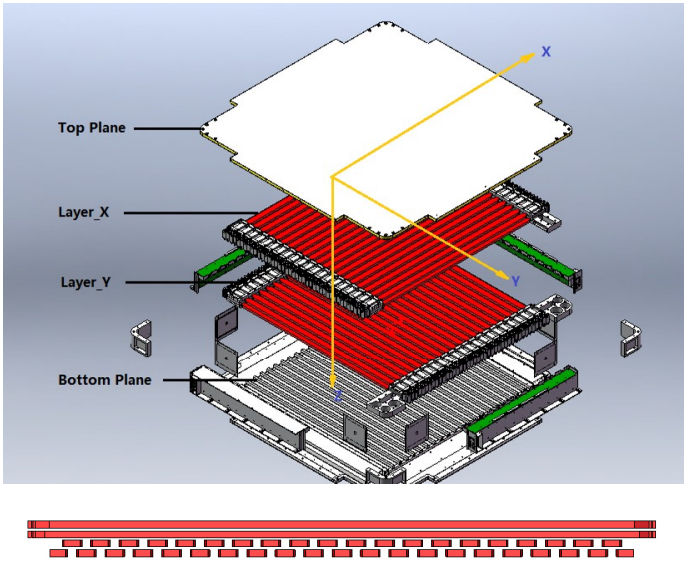

Fig. 1 The arrangement of PSD bars and the side view of PSD bars.

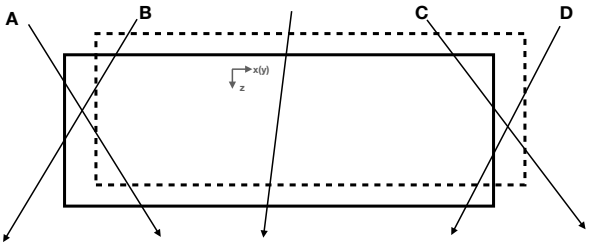

Fig. 2 Schematic view of a misaligned PSD bar. The *dashed* and *solid rectangles* represent the expected and real positions of a PSD bar respectively. The four event types (A, B, C and D) passing through a corner of the PSD bar can be used to correct for misalignment, thanks to the dependence of PL on bar misalignment.

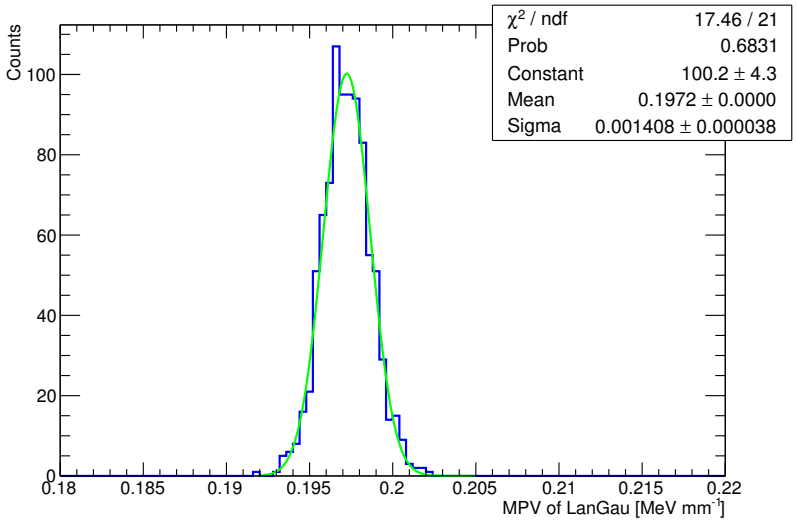

Fig. 3 MPV distribution of 902 segments for all PSD bars, where the MIP events are limited to pass in the middle region of the PSD bar in Fig. 2. It is credible that these events are affected negligibly by H, V and θ_{xy}.

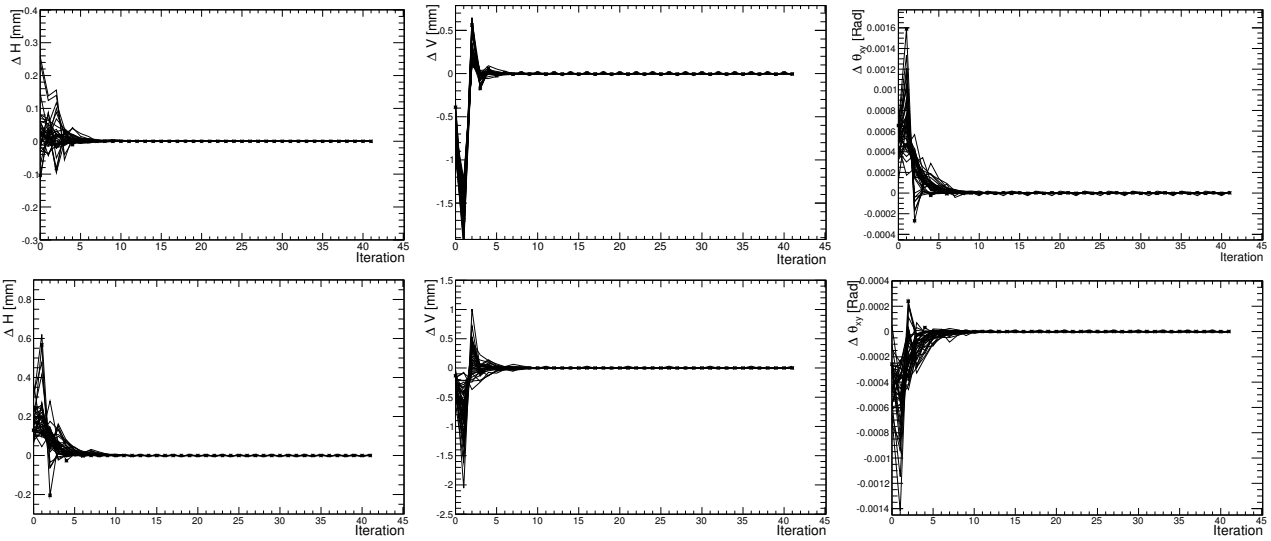

Fig. 4 Convergence of parameter variations with iteration. The first and second rows show convergence trends of the first PSD layer and the second PSD layer, respectively. Left, middle and right plots correspond to H, V and θ_{xy} respectively.

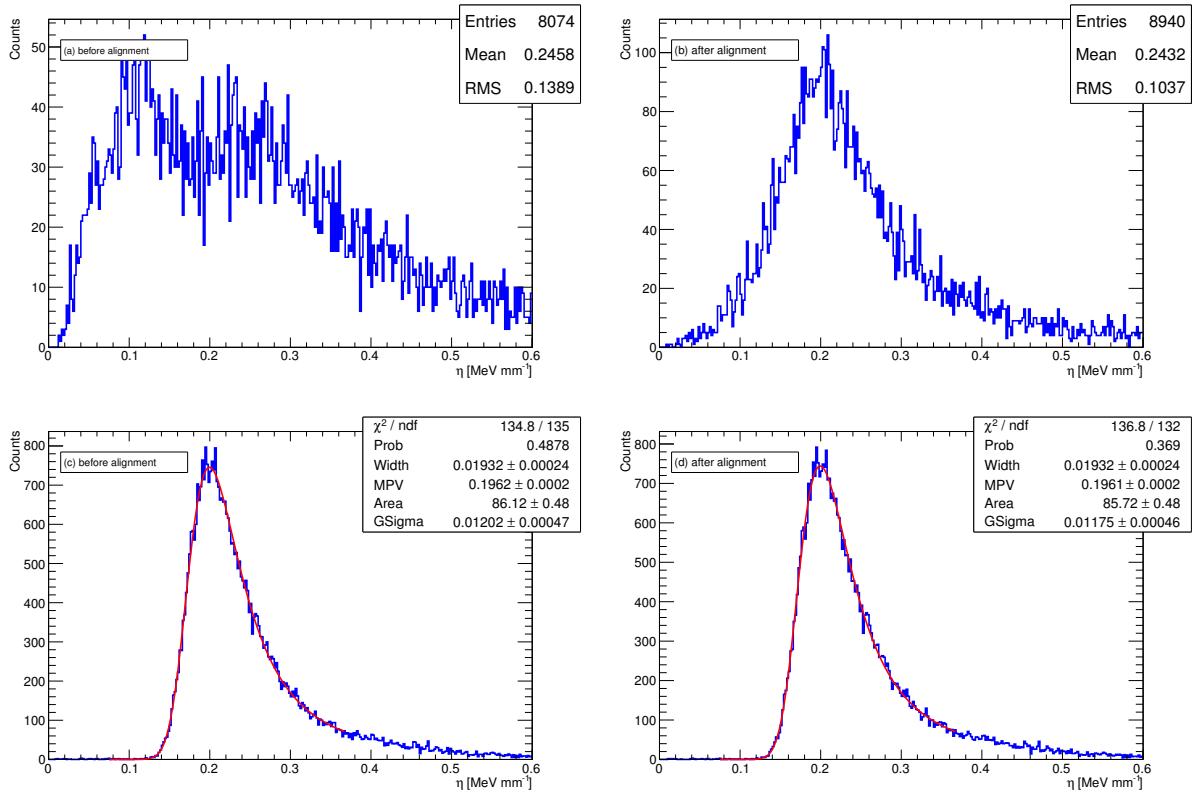

Fig. 5 The η distribution of MIP events passing through the 6th segment of the 23rd PSD bar in the first layer. Four cases are shown: corner events before (a) and after (b) the alignment, and middle events before (c) and after (d) the alignment. The *red lines* correspond to the fit with a Landau distribution convolved with a Gaussian function (*Color version is online*).

At the same time, we define the deposited energy per millimeter ($\mathrm{MeV\,mm^{-1}}$) as η in this paper. As mentioned above, three alignment parameters need to be calibrated: horizontal shift (H), vertical shift (V) and rotation angle in the xy plane (θ_{xy}). The track of a charged particle is a 3D line given by the STK. It is defined by a space point (P_x, P_y, P_z) and a direction vector (D_x, D_y, D_z).

The angle between the track and z axis is defined as $\theta = \arctan\left(\sqrt{D_x^2 + D_y^2}/D_z\right)$.

If a PSD bar has a shift or rotation, we import three misalignment parameters and get new positions for four surfaces of each PSD segment. We use the track information from STK to calculate the PL by $\frac{\Delta z}{\cos\theta}$ because θ_{xz} and θ_{yz} can be ignored. The real PL is different from the ideal PL and the real PL can be calculated as

$$\begin{aligned} &PL(H, V, \theta_{xy}) = \\ &\frac{1}{\cos\theta} \cdot \left(a\frac{D_z}{D_{x(y)}} H - aV + a\frac{D_z}{D_{x(y)}} \Delta L_i \theta_{xy} - P_z \right. \\ &\left. + a\frac{D_z}{D_{x(y)}} \left(x_0(y_0) + b\frac{W}{2} - P_{x(y)} \right) - az_0 + \frac{T}{2} \right), \end{aligned} \tag{2}$$

where ΔL_i is the offset along the bar of the i-th segment with respect to the center of a bar, (x_0, y_0, z_0) is the ideal geometrical center point of one PSD bar, and T and W are, respectively, the thickness and width of a PSD bar. $a = -1$ for cases A and D, see Figure 2, and $a = 1$ for cases B and C; $b = -1$ is for cases A and B, and $b = 1$ for cases C and D.

After substituting Equation (2) into Equation (1), for each corner event we get

$$H - \frac{D_{x(y)}}{D_z} V + \Delta L_i \theta_{xy} = C, \tag{3}$$

where

$$\begin{aligned} C = &\frac{D_{x(y)}}{D_z} \left(\frac{aE_{\rm dep}\cos\theta}{S} + z_0 + aP_z - a\frac{T}{2} \right) \\ &+ P_{x(y)} - x_0(y_0) - b\frac{W}{2}. \end{aligned} \tag{4}$$

For all corner events we obtain the following matrix equation

$$\begin{pmatrix} 1 & \left[-\frac{D_{x(y)}}{D_z}\right]_1 & [\Delta L_i]_1 \\ 1 & \left[-\frac{D_{x(y)}}{D_z}\right]_2 & [\Delta L_i]_2 \\ \vdots & \vdots & \vdots \\ 1 & \left[-\frac{D_{x(y)}}{D_z}\right]_N & [\Delta L_i]_N \end{pmatrix} \begin{pmatrix} H \\ V \\ \theta_{xy} \end{pmatrix} = \begin{pmatrix} [C]_1 \\ [C]_2 \\ \vdots \\ [C]_N \end{pmatrix}, \tag{5}$$

where N is the number of corner events in the alignment data sample and the matrix has a least squares solution for (H, V, θ_{xy}).

We iteratively look for the least squares solution of the above matrix equation for (H, V, θ_{xy}) as follows:

Step 1: construct the matrix from the corner-passing events, and then find the least squares solution;

Step 2: use (H, V, θ_{xy}) to calculate the aligned geometry;

Step 3: use the aligned geometry to construct the matrix (Eq. 5) and generate the updated least squares solution $(H + \delta H, V + \delta V, \theta_{xy} + \delta\theta_{xy})$;

Step 4: repeat steps 1–3 until $|\delta H| < 1\,\mu\text{m}, |\delta V| < 1\,\mu\text{m}$ and $|\delta\theta_{xy}| < 10\,\mu\text{rad}$.

Every variable is set to zero before alignment. After less than about 15 iterations we get the final alignment constants (H, V, θ_{xy}), and the most significant convergences always appear in the first step, as seen in Figure 4.

3 VALIDATION OF ALIGNMENT AND IMPROVEMENT OF CHARGE RESOLUTION

Due to the shift and rotation, the PL of MIP events within a PSD bar will be calculated incorrectly if no alignment is performed. As a result, a double-peak structure in the η distribution for corner events is observed in all PSD bars. Figure 5(a) displays a typical result for a PSD bar which also demonstrates that precise alignment is required. The η distributions in Figure 5 are fitted with a Landau distribution convolved with a Gaussian function. Based on the alignment methodology in Section 2, η is re-calculated iteratively. Results indicate the double peak structures of corner events are effectively eliminated and the charge resolution of proton MIP events is improved about 1.3 times, as shown in Figure 5(b). Meanwhile, the change in η spectra for middle events before and after the PSD alignment is minor. Fit results in Figure 5(c) and (d) show that the η spectrum of the middle events does not improve after the alignment.

These alignment parameters for the PSD will be used to reconstruct data during the whole lifetime of the DAMPE mission. Considering that plastic can dramatically change its geometry depending on temperature (Zhang et al. 2017; Li et al. 2017), we also studied the stability of the alignment parameters with time because the angle of sunlight changes seasonally, causing temperature variation. In this procedure, we divided one year of data into four groups, with a step of 3 months. MIP events in a different time range can be used to get the alignment parameters, and the variations of these four groups are displayed in Figure 6. Almost all of the alignment parameters for PSD bars change only slightly except for the few bars located at the edge of the PSD detector. This edge fluctuation is caused by lower statistics of corner segments, due to the lower geometrical acceptance of the BGO trigger for the border events.

Figure 7 depicts the alignment parameters after applying our method: the horizontal shift is relatively small, [–0.18 mm∼0.56 mm] for the first layer and

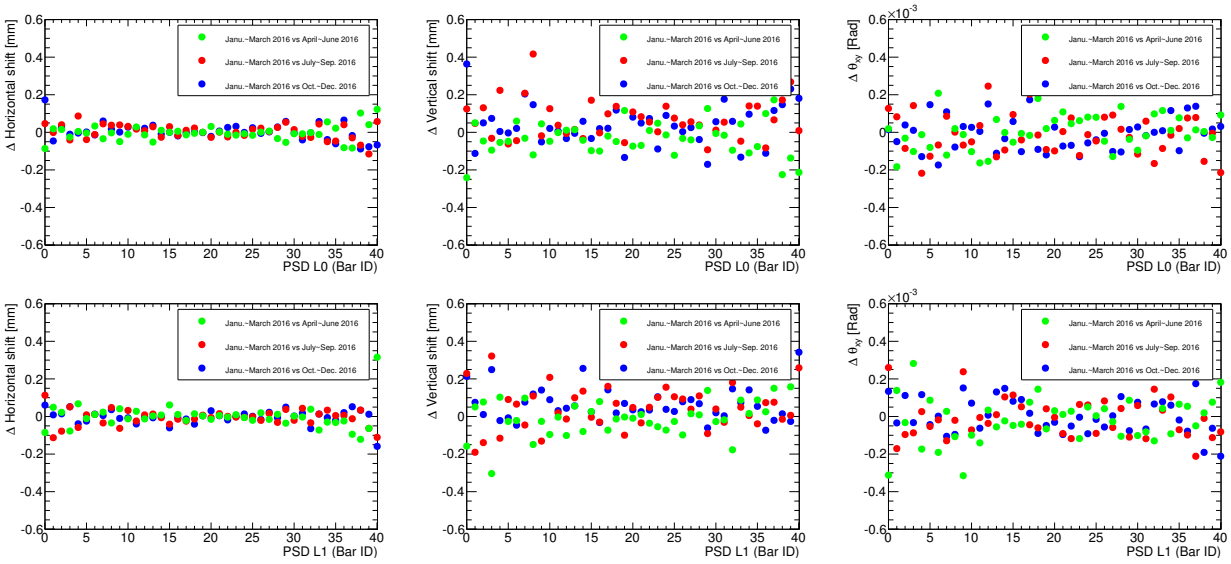

Fig. 6 Variations of misalignment parameters at different times. Each *filled circle* represents one PSD bar. The *green ones* indicate variations between Jan. 2016 – Mar. 2016 and Apr. 2016 – June 2016, the *red ones* mean variations between Jan. 2016 – Mar. 2016 and July 2016 – Sep. 2016, and the *blue ones* signify variations between Jan. 2016 – Mar. 2016 and Oct. 2016 – Dec. 2016. The two rows are for the PSD's first layer and second layer, respectively. The three columns from left to right correspond to variations of H, V and θ_{xy}, respectively.

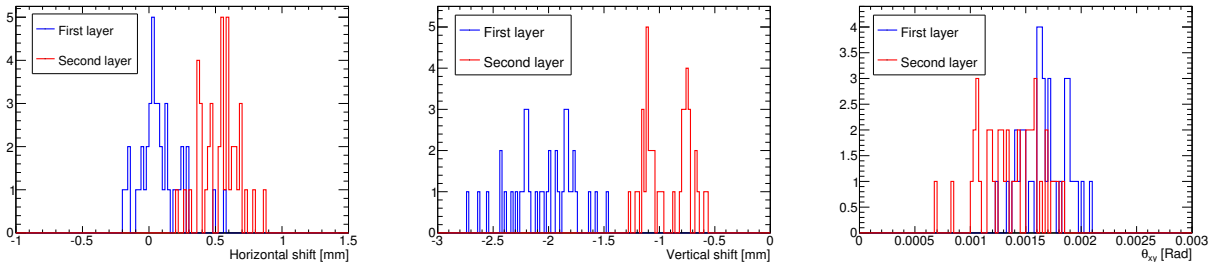

Fig. 7 Distributions of the alignment parameters, with the three columns corresponding to H (left), V (middle) and θ_{xy} (right). The *blue* and *red histograms* indicate the first and second layers respectively.

[0.27 mm∼0.79 mm] for the second layer. The two layers of PSD are shifted up, [–1.57 mm ∼–2.63 mm] for the first layer and [–0.56 mm∼–1.26 mm] for the second layer. The rotation is counterclockwise and the mean angle is about 0.0015 rad. The vertical shift is dominant.

To validate the alignment procedure, we manually import position shifts and rotations that come from the real geometry to the PSD geometry in the Geant4 Monte Carlo simulation, then the same alignment method is applied to the misaligned Monte Carlo sample. In Figure 8 we plot all the alignment variables H, V and θ_{xy} extracted for each PSD bar. There is an overall good agreement between initial values and calculated ones.

Based on DAMPE first-year data, we reconstruct the charge spectrum from H to Fe, as seen in Figure 9 (Dong et al. 2019), where the green line is the charge spectrum before the alignment, and the red one is after the alignment. As can be seen in the figure, the charge resolution for all nuclei improves significantly, especially for high abundance elements like H, He, C, N, O and Fe. Quantitatively, we summarize the charge resolution for several nuclei in Table 1. After the alignment, charge resolution is improved by 4%–8%.

4 RESULTS AND POSSIBLE APPLICATION

We present a method to align the DAMPE PSD detector. Our main goal is to obtain information about the real PSD detector geometry, which will be then applied to data acquired from DAMPE. In particular, a precise PSD alignment is crucial for the measurement of cosmic ray nuclei flux. With help from the η distribution for middle and corner events, shifts and rotations of PSD bars can be extracted natively and then integrated into the designed PSD

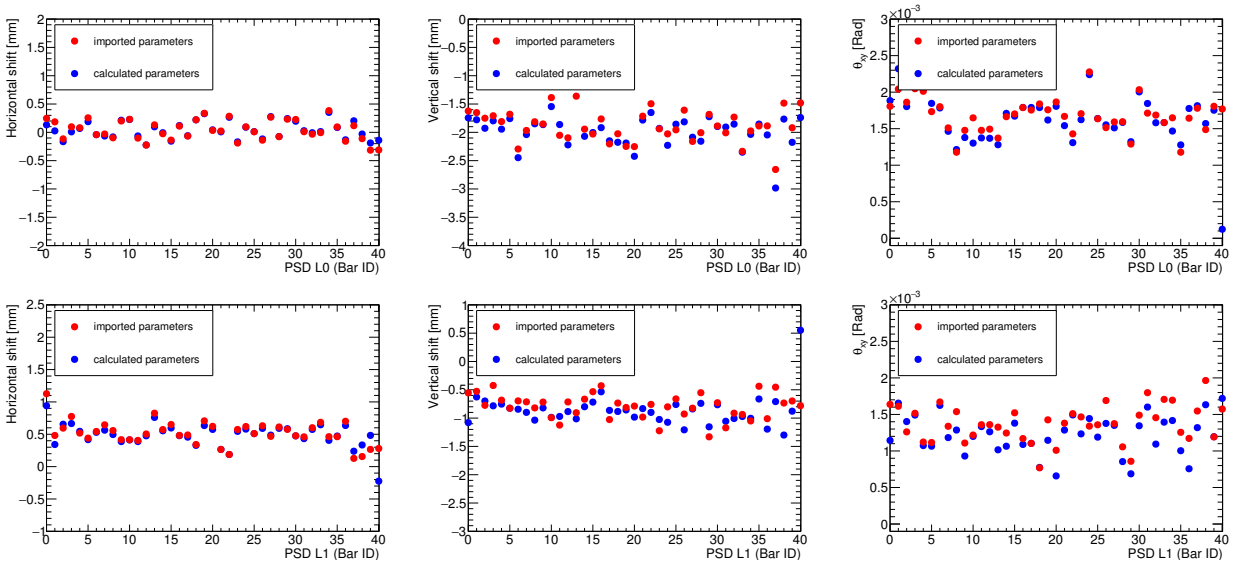

Fig. 8 Validation of the alignment with muon Monte Carlo samples: *red dots* represent the misalignment parameters applied to the samples, while *blue dots* are the alignment parameters calculated for these samples using our method. The first and second rows correspond to the first and second PSD layers respectively. The left, middle and right columns signify H, V and θ_{xy} respectively.

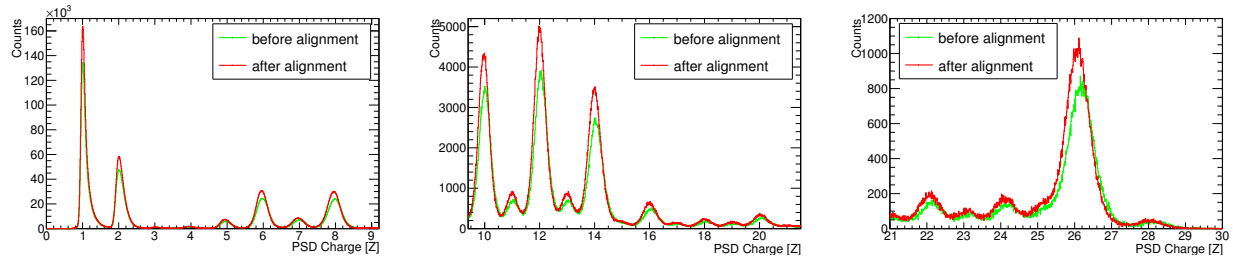

Fig. 9 The comparison of PSD charge spectrum: the *red line* is PSD charge with alignment correction and the *green one* shows the charge without alignment correction. One can see the significant improvement of charge resolution, which is particularly important for the physical analysis of cosmic rays.

Table 1 Improvement of charge resolution after applying the PSD alignment correction. The charge resolution corresponds to either a width of a Landau fit ($Z = 1, 2$) or σ of a Gaussian fit ($Z > 2$).

Element	H	He	Li	Be	B	C	O	Ne	Mg	Si
Before	0.037	0.056	0.126	0.124	0.138	0.156	0.202	0.239	0.254	0.286
After	0.035	0.051	0.119	0.119	0.131	0.149	0.193	0.229	0.240	0.274
Improvement	5.4%	8.9%	5.5%	4.0%	5.1%	4.5%	4.5%	4.2%	5.5%	4.2%

geometry. After performing the alignment, we compare the η distribution both for the middle and corner events, before and after the alignment. Thanks to the alignment procedure, the apparent distortion of the η distribution for the corner events is eliminated, demonstrating a high efficiency for the alignment method. Due to the improved charge resolution after the PSD alignment, the presented result is expected to significantly reduce the systematic uncertainty in measurement of cosmic ray nuclei flux.

Our alignment method is significantly different from the traditional detector alignment used in STK alignment (e.g. Tykhonov et al. 2018). Traditionally, a precise track can be reconstructed and the residual between expected and calculated position can serve as a good quantity for performing the alignment. This traditional method cannot be easily applied in the case of PSD, since PSD bars have considerable size. On the other hand, the MPV of the MIP signal reflects the PL of a particle track and can be precisely measured. Therefore, we show that the signal amplitude is a quantity which can be successfully used to perform the alignment. Our alignment method certainly first requires a precise track. Finally, we believe that our methodology can be successfully applied for the alignment of other large-scale detector units.

Acknowledgements We thank A. Tykhonov for helpful feedback on previous drafts. This work was funded by the National Key Program for Research and Development (2016YFA0400200), the Strategic Priority Research Program of the Chinese Academy of Sciences (XDB23040000) and the National Natural Science Foundation of China (Grant Nos. 11773086, U1738205, U1738127, 11673021, 11673047, 11673075, 11643011, 11773085, U1738207, U1738138, U1631111, U1738129 and 11703062).

References

Agostinelli, S., Allison, J., Amako, K. A., et al. 2003, Nuclear instruments and methods in physics research section A: Accelerators, Spectrometers, Detectors and Associated Equipment, 506, 250

Ambrosi, G., An, Q., Asfandiyarov, R., et al. 2019, Astroparticle Physics, 106, 18

Azzarello, P., Ambrosi, G., Asfandiyarov, R., et al. 2016, Nuclear Instruments and Methods in Physics Research A, 831, 378

Chang, J., Ambrosi, G., An, Q., et al. 2017, Astroparticle Physics, 95, 6

DAMPE Collaboration, Ambrosi, G., An, Q., et al. 2017, Nature, 552, 63

Ding, M., Zhang, Y., Zhang, Y.-J., et al. 2018, arXiv:1810.09901

Dong, T., Zhang, Y., Ma, P., et al. 2019, Astroparticle Physics, 105, 31

He, M., Ma, T., Chang, J., et al. 2016, Acta Astronomica Sinica, 57, 1

Li, Y., Zhang, Y. P., Zhang, Y. J., et al. 2017, Acta Astronomica Sinica, 58, 54

Tykhonov, A., Ambrosi, G., Asfandiyarov, R., et al. 2018, Nuclear Instruments and Methods in Physics Research A, 893, 43

Xu, Z.-L., Duan, K.-K., Shen, Z.-Q., et al. 2018, RAA (Research in Astronomy and Astrophysics), 18, 027

Yu, Y., Sun, Z., Su, H., et al. 2017, Astroparticle Physics, 94, 1

Yuan, Q., & Feng, L. 2018, Science China Physics, Mechanics, and Astronomy, 61, 101002

Zhang, Y., Zhang, Y., Dong, T., et al. 2017, International Cosmic Ray Conference, 35, 168

Zheng, L., Du, Y., Zhang, Z., et al. 2016, Nuclear Instruments and Methods in Physics Research A, 834, 98